Research Article

SOHAG JOURNAL OF SCIENCES

https://doi.org/10.21608/sjsci.2024.240208.1133

Synthesis, Characterization, and Electrochemical Analysis of Graphene Oxide Prepared by Modified Hummer's Method

Muhammad Abd El-Monema[1,*], Mohamed Khairy[2], Khaled G. Mahmoud[2], A. M. Abdel-Ghany[1], A. A. Ebnalwaled[3], and E. M. M. Ibrahim[4]

[1] *Basic Sciences Department, Faculty of Engineering, Sinai University, Egypt*
[2] *Chemistry Department, Faculty of Science, Sohag University, Sohag, 82524, Egypt*
[3] *Physics Department, Electronics and Nano Devices Lab, Faculty of Science, South Valley University, Qena 83523, Egypt*
[4] *Physics Department, Faculty of Science, Sohag University, Sohag 82524, Egypt*
[*] *Email: mohamed.mouniem@gmail.com*

Received: 7th October 2023 **Revised:** 12th December 2023 **Accepted:** 1st January 2024
Published online: 30th January 2024

Abstract: This work aims to explore the structural, morphological, and electrochemical features of graphene oxide. The study investigates graphene oxide's electrochemical behavior in supercapacitor applications. The graphene oxide was synthesized using the modified Hummer's method. XRD, Raman spectroscopy, and (HR-TEM) were used to investigate structural and morphological properties. The results confirmed the formation of the typical hexagonal structure of the graphene oxides. Raman spectrum showed two distinct G (primary mode of graphene) and D (defect or disorder mode) Raman modes at 1592 cm^{-1} and 1349 cm^{-1}, respectively, in addition to D+D' and 2D modes. The electrochemical measurement revealed that the GO electrode has a specific capacitance of 38.33 F/g at a current density of 5 A/g in a 1 M KOH electrolyte with a very low charge transfer resistance of 0.97Ω. These findings suggested that this straightforward method can be used to create various graphene-derived electrodes for upgrading current supercapacitors.
Keywords: Graphene oxide, Graphene, supercapacitor, Hummer's method, electrode material.

1. Introduction

Graphene, fullerene, carbon nanotubes (CNTs), and other carbon allotropes have various optoelectronic, electrical, thermal, and mechanical properties that make them unique materials [1–3]. Graphene and graphene derivatives, such as graphene oxide (GO) and reduced graphene oxide (rGO), have many remarkable features that endow them with feasibility for many fields of applications. These features include a large surface area, good optical transmittance, high electrical conductivity, chemical stability, a tunable band gap, biocompatibility, thermal conductivity, porosity, and high elasticity. Therefore, many researchers have been interested in exploring the potential of graphene and its derivatives [2,4]. Graphene is a nanomaterial that has a very thin and strong structure. It also has many amazing properties, such as Ballistic transport over long distances with electron mobility that is ten times higher than silicon, quantum confinement that causes the Coulomb blockade effect and a small band gap [5], the half-integral quantum Hall effect (at room temperature) [6], and massless relativistic quasiparticles (Dirac fermions) as charge carriers.

The double-layered capacitance feature of Graphene allows electrolyte charges or ions to be stored on both active and electrochemically stable materials with enormous surface areas. The optimization of surface properties that enhances the surface energy is the main approach for tuning the capacitive characteristics of carbon-based nanostructures. Also, the number of layers has a large influence on GO characteristics in particular. [7]. GO has a multilayer structure with several oxygen functional groups on its basal planes and edges. GO is hydrophilic due to these functional groups. As a result, GO disperses in water more easily than graphene. In the production of composites containing metal oxides/conducting polymers for high-performance supercapacitor applications, the solubility of GO whether in water or organic solvents, is crucial [1].

Moreover, GO is a novel nanomaterial consisting of carbon that can be derived from graphite. GO has potential applications in various nano-devices that can adjust their electronic, optical, thermal, and other properties according to specific conditions [8,9]. GO has outstanding features such as strong carrier thermal conductivity, mobility, and mechanical strength [10].

Due to their abundant oxygen functional groups and high surface area, these two-dimensional materials are suitable for further modification. These properties enable the GO structure to have broad application prospects in various domains such as photovoltaic [11], energy storage, catalysis [12], biosensors [13], and so on. GO provides a variety of chemical techniques for attaching various functional groups to its surface, allowing it to adjust its electrical, optical transparency, and thermal conductance [14]. Furthermore, by entirely adjusting its functional groups, it can modify its band gap to obtain zero band gap graphene. Because of the existence of oxygenated groups, the GO structure has attractive characteristics. These oxygenated groups have various advantages over graphene,

including better solubility, quicker production, and additional surface functionalization options in nanocomposite material applications [15].

GO has 30.2 F/g at a scan rate of 50 mV/s with 0.1 M tetraethylammonium tetrafluoroborate (TEABF4) in acetonitrile (CH3CN) as an electrolyte, as reported by P.T. Nam et al. [16]. Xiawei Yun. et al. reported that GO has a specific capacitance of 101 mF/cm^2 at a current density of 0.5 mA/cm^2 in PVA/H_3PO_4 gel electrolyte [17]. Thangappan, R. et al. reported that GO gas has a specific capacitance of 15.7 F/g at a current density of 1 A/g in a neutral aqueous electrolyte [18]. In the present work, the GO electrode has a specific capacitance of 38.33 F/g at a current density of 5 A/g in a 1 M KOH electrolyte with a very low charge transfer resistance of 0.97Ω.

However, some studies have suggested that graphene oxide is not suitable for supercapacitors, while others have shown that it can achieve high capacitance and stability when combined with other materials such as polymers or metal oxides [19]. To resolve this apparent contradiction, we conducted a study on the performance of graphene oxide as a supercapacitor electrode. We found that graphene oxide has excellent capacitive properties and may be a better option than other materials because of its higher capacitance, lower cost, and shorter processing time. Our work provides a new perspective for the design and synthesis of supercapacitor electrodes and other energy devices.

This work employs a modified Hummer's method to fabricate the GO. The samples were examined by XRD, TEM, and Raman to reveal their structural, morphological, and electronic properties, respectively. The electrochemical features of the synthesized GO sample were evaluated using the two-electrode system. This study demonstrates a simple and versatile approach to fabricating different types of electrodes based on graphene derivatives for enhancing the performance of existing supercapacitors. This implies that the proposed method has significant implications for the development of novel and efficient energy storage devices.

2. Materials and method

2.1. Chemicals

Graphite powder (Fisher Chemical UK Ltd.), hydrogen peroxide (H_2O_2), Sulfuric acid (H_2SO_4), acetone, hydrochloric acid (Piochem, Egypt LTD), and $KMnO_4$ (with a purity of 99% supplied from Riedel de Han) were employed without any additional refinement.

2.2. Material Synthesis

The synthesis of graphen oxide was performed using Hummer's method as described previously [20]. Briefly, a mixture of 1.0 g of graphite in powder and 50 mL of pure H_2SO_4 was stirred in an ice-water bath. Then, 6.0 g of $KMnO_4$ was added dropwise with continuous stirring for one hour at room temperature. Next, 80 mL of distilled water was gradually added to the mixture while the temperature was raised to 50 °C until the solution's color changed from light brown to dark brown. Then, in drops, 200 mL of distilled water and 6.0 mL of 30% hydrogen peroxide were added till the solution turned yellow from dark brown. The resultant GO was centrifuged, cleaned repeatedly with a 5% HCl/acetone solution, and finally dried for 12 hours at 65 °C under vacuum.

2.3. Materials characterization

The crystallinity and phase purity of GO were investigated using Bruker D8-Advance X-ray diffractometer with monochromatic CuKα radiation with wavelength λ= 1.5406 at 60 mA and 40 kV. Raman spectroscopy analyses were carried out using a Raman spectrometer (Model alpha300 R - Raman Imaging Microscope). The laser's power of the excitation source was 3.0 mW. For all spectra, the excitation wavelength was 532 nm. The sample was further examined using a (HR-TEM) model JEM 2100 from Tokyo, Japan.

2.4. Electrochemical measurements

The nanocomposite of GO was mixed with carbon black and PTFE in a weight ratio of 8:1:1. The mixture was then coated on a nickel foam with an area of 1.0 cm^2 and vacuum-dried at 50°C for half an hour. The electrochemical properties of the nanocomposite-modified nickel foam (NF) electrode, which had about 2 mg of GO, were investigated.

An electrochemical workstation (IVIUM Compact Stat.h10 potentiostat/galvanostat controlled by IVIUM software) with a potential varies between -0.3 to 0.4 V and 1.0 M KOH as an electrolyte in a two-electrode cell was utilized to study the galvanostatic charge-discharge (GCD) and cyclic voltammetry (CV) behaviors. The electrochemical impedance study was also conducted. The range of frequency was varied between 0.1 Hz to 100 kHz, at AC applied potential 10 mV. Thus, the specific capacitance (Csp) was derived from the GCD curve by applying the following equation:

$$C_{sp} = \frac{I\ x\ \Delta t}{m\ x\ \Delta V} \quad (1)$$

where I is the discharge current (A), Δt is the discharge time (s), m is the weight of the active material (g) and ΔV is the potential window (V).

3. Results:

3.1. Structural characterization:

XRD can identify the crystal structure as well as the crystallinity of the graphene that was prepared. The XRD pattern of GO as seen in Figure. 1. shows a prominent (001) reflection at the 9.30^0, related to a d-spacing of 0.95 nm, which is bigger than that of pure graphite of 0.34 nm because of the existence of functional groups that contain oxygen on the graphite layers [1]. Another broad reflection ws detthe ected at 42.2^0, which corresponded to a d-spacing of about 0.24 nm with the (100) plane.

The crystallite size (D) of the synthesized GO was determined using the Debye–Scherrer equation:

$$D = \frac{K\ \lambda}{\beta_{hkl}\ cos\ \theta} \quad (2)$$

Where K is a constant, λ is wavelength (1.5406 Å), β_{hkl} or FWHM is the full width of the diffraction peak at half maximum, and θ is the diffraction angle.

The dislocation density (δ) and the internal strain (ε) of GO were estimated using the following relations, respectively:

$$\delta = \frac{1}{D^2} \quad (3)$$

$$\varepsilon = \frac{\beta \cos\theta}{4} \quad (4)$$

The structural parameters of the prepared GO (tabulated in Table 1) are close to those previously reported in the literature [1].

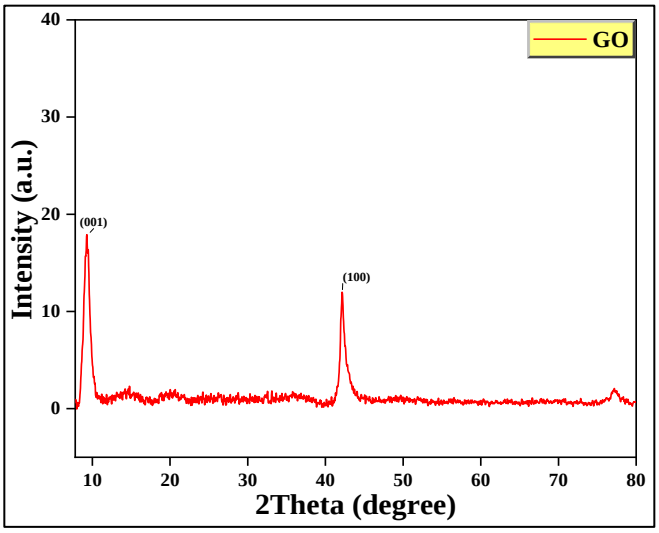

Fig. 1. XRD pattern of GO

Table 1. Diffraction angthetas) value, FWHM (β), cthe rystallite size (D), microstrain (ε) and dislocation density (δ) of graphene oxide.

2θ°	d-spacing (nm)	FWHM (β)	$\varepsilon \times 10^{-4}$	D(nm)	$\delta \times 10^{-4}$ (line/nm^2)
9.3	0.95	0.596778	3.2	13.35	0.65

The Raman spectrum can unveil the electronic, structural, and physical characteristics of carbon compounds. Figure. 2 illustrates the Raman spectrum of GO nanosheets. As seen, two distinct G and D bands are found at 1592 cm^{-1} and 1349 cm^{-1}, respectively where, the G band corresponds to the sp^2 carbon atoms' in-plane vibration and is associated with the E_{2g} phonons of the sp^{2}C atoms. Also, The D band is associated with the breathing mode corresponding to k-point phonons with A_{1g} symmetry and defect sites. These defects may arise from grain boundaries, vacancies, dislocations, and amorphous carbon [21–24]. The ratio between the D and G band intensities (ID/IG) measures the purity of the product. ID/IG was calculated to be 0.98 indicating good crystallinity of the synthesized GO. The Inset of Figure. 2 highlights the Raman spectrum within the range of Raman shift from 2500 to 3500 cm^{-1}. The data imply the appearance of two additional notable bands at 2762 and 2931 cm^{-1}, which denote the 2D and D+D' bands, respectively. The 2D mode denotes the two-phonon double resonance Raman technique and is used to identify the graphene layer stacking order [24]. Meanwhile, the D+D' band represents a second-order band resulting from the combination of the D and G modes [25]. The position of the 2D band (at 2762 cm^{-1}) suggests the multilayered structure of the produced GO, as the 2D band of monolayer GO typically appears at 2679 cm^{-1} [26]. Furthermore, the value of (IG/I2D) for GO is 1.065, confirming its multilayered nature [27–29]. Additionally, the broadness of the 2D band suggests that the synthesized graphene possesses a few layers with some imperfections[30].

3.2. Morphological study:

TEM has been applied to GO since its discovery [31] and is one of the most effective methods to examine its surface composition. The TEM images of the synthesized GO (Figure. 3) reveal a two-dimensional clear sheet of GO with wrinkles and scroll regions resulting from the overlapping of several layers. Additionally, the image shows that the edges of the GO sheet are folded [31–33].

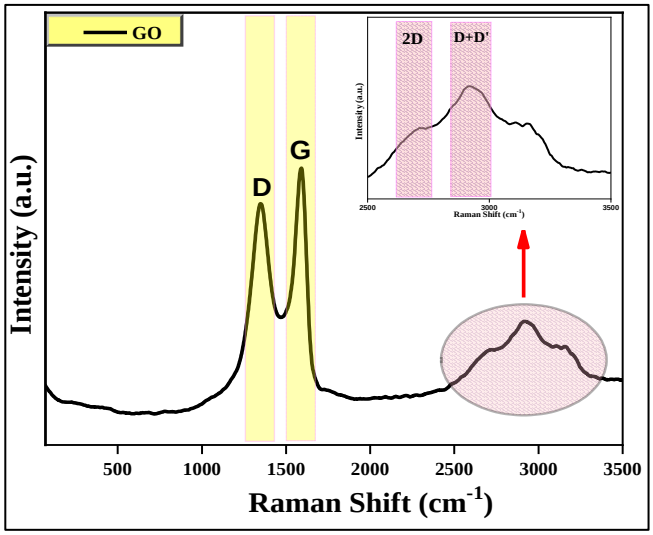

Fig. 2. Raman Spectra of GO

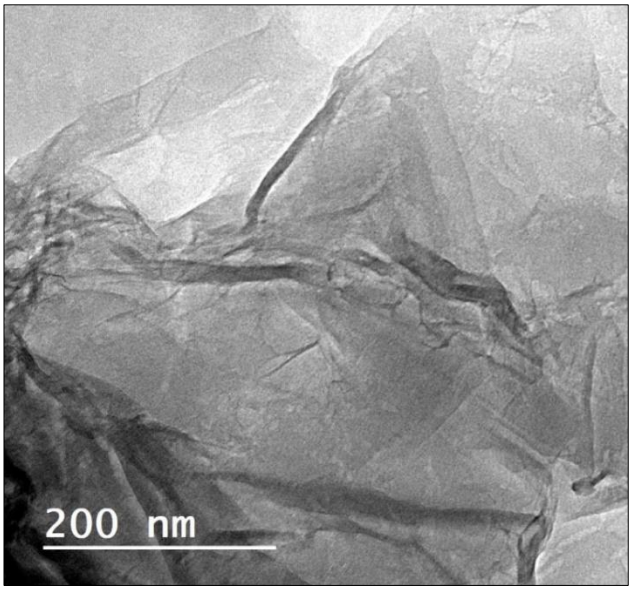

Fig. 3. TEM image of GO

3.3. Electrochemical Analysis:

The performance of a supercapacitor device using GO nanocomposite was studied using CV, GCD, and EIS. The CV method can be used to study the role of material in

supercapacitor applications by analyzing the performance at different scan rates. Also, CV curves can be used to identify the redox behavior resulting from the pseudocapacitance material [34]. Figure. 4. shows the CV curves of GO nanocomposite at various scan rates. According to the theory, the CV curves for the perfect capacitor should be rectangular loops due to the high resistance and low contact resistance [34]. On the other hand, the peaked shape of CV curves is considered a sign of pseudocapacitance material [35]. The GO electrode shows redox peaks between -0.3 and 0.4 V, attributed to its psedocapacitance nature due to the attached oxygen-containing functional groups on its basal planes [19]. This result also supports the idea that the charge storage resulted from the battery-type pseudocapacitive behavior of the prepared GO [36,37]. The CV curves become more distinct and have larger areas as the scan rate increases. The peak of current density also increases with the scan rate, showing a good ion response and enhanced capacitance behavior. Moreover, the higher scan rate causes higher current density, which indicates that the electrode material has more conductivity, less internal resistance, and good capability in the 1 M $KMnO_4$ electrolyte [38,39]. The similar shape of CV curves at different scan rates of 50-200 mV/s suggests that the electrode has a fast faradic reaction [39,40].

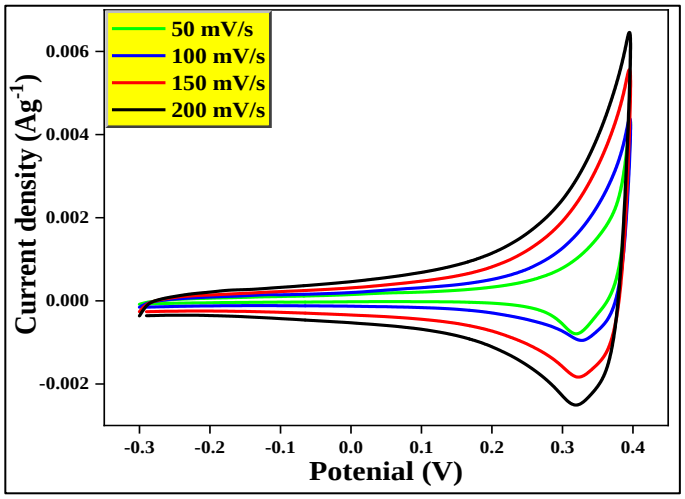

Fig. 4. CV curves of GO at different scan rates.

The galvanostatic charge-discharge curve depicted in Figure. 5 was employed to estimate the specific capacitance of the produced GO nanomaterial. At a current density fixed at 5 A/g, the electrode has a specific capacitance of 38.33 F/g.

By applying electrochemical impedance spectroscopy (EIS), the electrochemical performance, electrical conductivity, and charge transport properties are further investigated. The EIS is conducted in the frequency range of 0.1 Hz to 100 kHz, with an AC potential of 10 mV in a 1 M KOH electrolyte. EIS explores the basic behavior of electrode materials. The Nyquist plot of a GO nanocomposite in Figure. 6 displays a linear segment in the region of low frequencies, which is the Warburg impedance (ZW), which is related to ion diffusion through the electrolyte and into the electrode surface; in the region of high-frequency, a slight semicircle loop is generated; this loop represents the resistance of charge-transfer (Rct), which reveal that the electrode has a weak internal resistance [41]. Weak internal resistance would decrease the loss of energy as undesired heat during the charging and discharging cycle in energy storage devices [42]. The semicircle of Rct of GO is shown in the inset of Figure.6. The semicircle in the GO Nyquist plot is incomplete, and the impedance exhibits a linear trend in the high frequency region, indicating a low internal resistance of the material. GO has an Rct of 0.97Ω. To match the impedance results of the GO, an equivalent circuit (Figure. 6) is proposed. The constant phase element (CPE) is around 0.012, and the Warburg impedance (ZW) is around 0.002688.

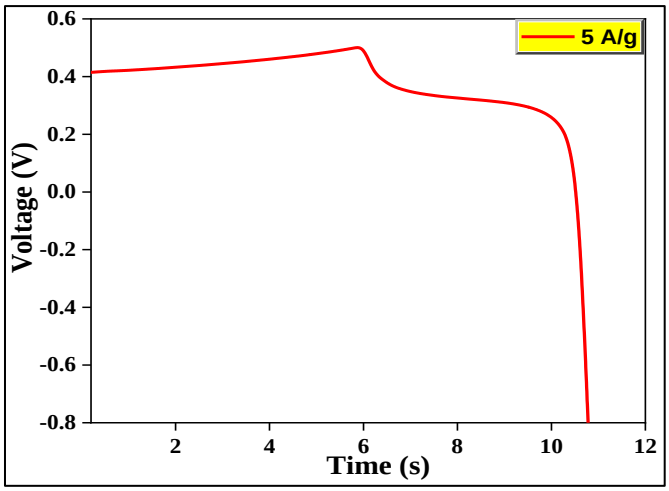

Fig. 5. GCD Curve of GO at scan rate of 5 A/g

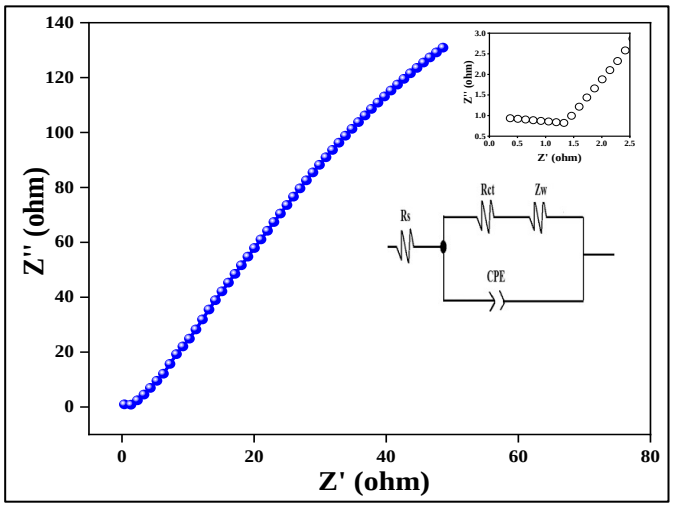

Fig. 6. Nyquist plots of GO nanocomposite.

4. Conclusion

Graphene oxide has been successfully prepared for use as an electrode for a supercapacitor using Hummer's method. The XRD, Raman spectroscopy, and HR-TEM were performed to identify the structure and morphology of the prepared sample. The XRD pattern revealed that the diffraction peaks correspond to GO without observation of any impurities. The Raman spectroscopy confirmed the formation of pure GO, with more details about the electronic and structural information. The HR-TEM revealed and confirmed the good crystallinity of GO. The

electrochemical characterizations of the GO electrode were performed by CV, GCD, and EIS techniques. The CV curves of the GO had a quasi-rectangular shape as an indication of good capacitive behavior and less contact resistance. The GCD curve was used to determine the specific capacitance of the GO electrode, which had a value of 38.33 F/g in a 1 M KOH as an electrolyte at a current density of 5 A/g. GO showed a small charge transfer resistance of 0.97Ω. This straightforward method can be used to create various graphene-derived electrodes for upgrading current supercapacitors.

CRediT authorship contribution statement:

Muhammad Abd El-Monem: Sample synthesis and characterization, analysess, calculations, writing the original draft, data presentation. Mohamed Khairy: electrochemical measurement and data analyse. Khaled G. Mahmoud: Investigation. M. Abdel Ghany: Writing - Review & Editing. A. A. Ebnalwaled: Supervision, resources, methodology. E.M.M. Ibrahim: main supervision, Writing - Review & Editing, Project administration.

Data availability statement

The data used to support the findings of this study are available from the corresponding author upon request.

Declaration of competing interest

The authors declare that they have no known competing financial interests or personal relationships that could have appeared to influence the work reported in this paper.

References

[1] H. Wang, L. Cui, Y. Yang, H.S. Casalongue, J.T. Robinson, Y. Liang, Y. Cui, H. Dai, *Journal of the American Chemical Society*, 132 (2010) 13978-13980.

[2] M. Civas, M. Kuscu, O.Cetinkaya, B.E. Ortlek, O.B. Akan, *APL Mater*, 11 (2023) 080901.

[3] A.K.& I. Ahmad, *Mater. Res. Innov*, 0 (2023) 1-15.

[4] S. Ghosh, K. Chatterjee, *Int. J. Nanomedicine*, 15 (2020) 5991–6006.

[5] Z. Zheng, X. Zu, Y. Zhang, W. Zhou, *Mater. Today Phys*, 15 (2020) 100262.

[6] V.S. Prudkovskiy, Y. Hu, K. Zhang, Y. Hu, P. Ji, G. Nunn, J. Zhao, C. Shi, A. Tejeda, D. Wander, A. De Cecco, C.B. Winkelmann, Y. Jiang, T. Zhao, K. Wakabayashi, Z. Jiang, L. Ma, C. Berger, W.A. de Heer, *Nat. Commun*, 13 (2022) 7814.

[7] G.O. Com-, N. Theophile, H.K. Jeong, H.K. Jeong, *Chemical Physics Letters* 669 (2016) 125-129.

[8] M. Shahbazi, A. Taherkhani, *Opt. Mater*, 123(2022)111849.

[9] X.M. Huang, L.Z. Liu, S. Zhou, J.J. Zhao, *Front. Phys*, 15 (2020) 33301.

[10] H. Alamgholiloo, S. Rostamnia, N.N. Pesyan, *Colloids Surfaces A Physicochem. Eng. Asp*, 602 (2020) 125130.

[11] E. Widianto, Shobih, E.S. Rosa, K. Triyana, N.M. Nursam, I. Santoso, *Opt. Mater*, 121 (2021) 111584.

[12] E. Doustkhah, S. Rostamnia, *J. Colloid Interface Sci*, 478 (2016) 280–287.

[13] X. Kang, R. Wang, M. Jiang, E. Li, Y. Li, T. Wang, Z. Ren, *Sensors and Actuators Reports*, 5 (2023) 100139.

[14] A.T. Dideikin, A.Y. Vul', *Front. Phys*. 6 (2019) 149.

[15] C.S. Tshangana, A.A. Muleja, A.T. Kuvarega, T.J. Malefetse, B.B. Mamba, *J. Water Process Eng*, 43 (2021) 102249.

[16] P.T. Nam, N. Van Khanh, N.T. Thom, N.T. Phuong, N. Van Trang, N.T. Xuyen, V.Q. Thai, V.A. Tuan, D.T. Mai Thanh, *Vietnam J. Chem*, 56 (2018) 778–785.

[17] X. Yun, B. Lu, Z. Xiong, B. Jia, B. Tang, H. Mao, T. Zhang, X. Wang, *RSC Adv*, 9 (2019) 29384–29395.

[18] R. Thangappan, S. Kalaiselvam, A. Elayaperumal, R. Jayavel, M. Arivanandhan, R. Karthikeyan, Y. Hayakawa, *Dalt. Trans*, 45 (2016) 2637–2646.

[19] B. Xu, S. Yue, Z. Sui, X. Zhang, S. Hou, G. Cao, Y. Yang, *Energy Environ. Sci.* 4 (2011) 2826–2830.

[20] W.S.. O. Hummers R., E., *J. Am. Chem. Soc*, 208 (1957) 1937.

[21] F.T. Johra, J.W. Lee, W.G. Jung, *J. Ind. Eng. Chem*, 20 (2014) 2883–2887.

[22] Fang, Peijiao, Mulligan, C.P., Jia, Ru, Shi, Jian, Khare, S.V., & Gall, Daniel, *Acta Materialia*, 266 (2022) 117643

[23] Y. Liu, Y. Zhang, G. Ma, Z. Wang, K. Liu, H. Liu, *Electrochim. Acta*, 88 (2013) 519–525.

[24] N.M.S. Hidayah, W.W. Liu, C.W. Lai, N.Z. Noriman, C.S. Khe, U. Hashim, H.C. Lee, AIP Conf. Proc. 1892 (2017).

[25] A.Y. Lee, K. Yang, N.D. Anh, C. Park, S.M. Lee, T.G. Lee, M.S. Jeong, *Appl. Surf. Sci*, 536 (2021) 147990.

[26] H. Liu, Y. Wang, X. Gou, T. Qi, J. Yang, Y. Ding, *Mater. Sci. Eng. B*, 178 (2013) 293–298.

[27] Y. Hwangbo, C.K. Lee, A.E. Mag-Isa, J.W. Jang, H.J. Lee, S.B. Lee, S.S. Kim, J.H. Kim, *Carbon N. Y*, 77 (2014) 454–461.

[28] T. Cui, S. Mukherjee, C. Cao, P.M. Sudeep, J. Tam, P.M. Ajayan, C. Veer Singh, Y. Sun, T. Filleter, *Int. J. Refrig*. 43 (2014) 36–49.

[29] M. Singh, H.S. Jha, P. Agarwal, *Mater. Lett*, 126 (2014) 249–252.

[30] F.T. Johra, J.W. Lee, W.G. Jung, *J. Ind. Eng Chem*, 20 (2014) 2883–2887.

[31] M.S. Amir Faiz, C.A. Che Azurahanim, S.A. Raba'ah, M.Z. Ruzniza, *Results Phys*, 16 (2020) 102954.

[32] P. Bampoulis, K. Sotthewes, E. Dollekamp, B. Poelsema, *Surf. Sci. Rep*. 73 (2018) 233–264.

[33] K.J. Goswami, N. Sen Sarma, *ACS Omega*, 8(2023)21914–21928.

[34] N.A. Mohd Zaid, N.H. Idris, *Sci. Rep*, 6 (2016) 3208.

[35] Y. Jiang, J. Liu, *Energy Environ. Mater*, 2 (2019) 30–37.

[36] D. Prakash, S. Manivannan, *J. Alloys Compd*, 854 (2021) 156853.

[37] O. Okhay, A. Tkach, *Nanomaterials*, 11 (2021) 1240.

[38] P. Xiong, C. Hu, Y. Fan, W. Zhang, J. Zhu, X. Wang, *J. Power Sources*, 266 (2014) 384–392.

[39] S. Ishaq, M. Moussa, F. Kanwal, M. Ehsan, M. Saleem, T.N. Van, D. Losic, *Sci. Rep*, 9 (2019) 1–11.

[40] J. Hao, J. Wang, S. Qin, D. Liu, Y. Li, W. Lei, *J. Mater. Chem. A*, 6 (2018) 8053–8058.

[41] G. Xiong, P. He, B. Huang, T. Chen, Z. Bo, T.S. Fisher, *Nano Energy*, 38 (2017) 127–136.

[42] S. Ahankari, D. Lasrado, R. Subramaniam, *Mater. Adv*, 3 (2022) 1472–1496.